

Journal of Materials Chemistry A

Materials for energy and sustainability

Accepted Manuscript



This is an Accepted Manuscript, which has been through the Royal Society of Chemistry peer review process and has been accepted for publication.

Accepted Manuscripts are published online shortly after acceptance, before technical editing, formatting and proof reading. Using this free service, authors can make their results available to the community, in citable form, before we publish the edited article. We will replace this Accepted Manuscript with the edited and formatted Advance Article as soon as it is available.

You can find more information about Accepted Manuscripts in the [Information for Authors](#).

Please note that technical editing may introduce minor changes to the text and/or graphics, which may alter content. The journal's standard [Terms & Conditions](#) and the [Ethical guidelines](#) still apply. In no event shall the Royal Society of Chemistry be held responsible for any errors or omissions in this Accepted Manuscript or any consequences arising from the use of any information it contains.

ARTICLE

Performance Optimization and Fast Rate Capabilities of Novel Polymer Cathode Materials through Balanced Electronic and Ionic Transport

Received 00th January 20xx,
Accepted 00th January 20xx

DOI: 10.1039/x0xx00000x

Cara N. Gannett^a, Brian M. Peterson^a, Luis Melecio-Zambrano^a, Colleen Q. Trainor^a, Brett P. Fors^{*a}, Héctor D. Abruña^{*a}

The increasing demands for high-power electrical energy storage technologies require the development of new electrode materials and architectures with fast ion and electron transport. Herein, we report a new family of ter-polymers as battery cathode materials which exhibit significantly improved performance over their parent co-polymers: poly(phenylene-phenazine), and poly(1,3,5-phenylene-phenazine). The high electronic conductivity of poly(phenylene-phenazine) and fast ionic transport of poly(1,3,5-phenylene-phenazine) are combined in this series of ter-polymers, exhibiting improved battery performances which are especially apparent at high rates. The optimized ter-polymer delivers 180 mAh g⁻¹ when discharged at 16 A g⁻¹, demonstrating the effectiveness of balancing ionic and electronic transport properties.

Introduction

The demand for lithium ion (Li-ion) batteries has grown dramatically in recent years in response to the electrification of transportation and growth in the mobile electronics sector.¹ To sustain such increasing demands, improvements in Li-ion battery technologies must be made to address limitations related to battery costs, accessibility of constituent elements, energy and power densities, and rate capabilities.^{2,3} Meeting these needs necessitates the development of new, sustainable, low cost electrode materials which can meet the increasingly high energy and power density requirements of emerging technologies.

Organic electrode materials have recently generated increased interest due to their natural abundance, reduced cost, greener synthetic methods, and easily tunable structures and properties.^{4–6} Further, organic materials are held together by weak intermolecular forces which can enable faster ionic transport and improved rate capabilities.^{7,8} However, organic materials often suffer from poor electronic conductivities and require high ratios of conductive additives (up to 80% by weight) in the electrode composite, limiting the energy/power densities of the resulting cells and their practical applicability.^{9–11} While highly conjugated materials with good π orbital overlap have demonstrated improvements in electronic conductivity, their rigid, ordered structures often limit ionic transport.^{12–17}

Herein, we present a new family of polymeric materials which enable high rate capabilities from balanced ionic and electronic conductivities. At a rate of 16 A g⁻¹, the optimized material delivers 180 mAh g⁻¹ when utilizing only 30% carbon additives by weight in the composite. When the carbon additives are further reduced to 10%, the material can still deliver 88 mAh g⁻¹ under a 16 A g⁻¹ load, demonstrating the exceptional power capabilities of the polymer.

Experimental

General Procedure for Polymer Synthesis

5,10-dihydrophenazine, 1,4-dibromobenzene, 1,3,5-tribromobenzene, sodium *tert*-butoxide, RuPhos Pd G2, and RuPhos ligand were charged to a Schlenk tube. After establishing a nitrogen atmosphere, toluene (5 mL) was added, and the reaction was stirred at 110 °C for 16 hours. The reaction was cooled, suspended in dichloromethane (100 mL), and washed with water (100 mL) five times, or until all sodium bromide was removed as shown by powder x-ray diffraction (XRD). Specific molar ratios, yields, and elemental analysis results can be found in the supporting information.

Coin Cell Fabrication

The polymers were studied for their electrochemical properties using CR 2032 Li metal half cells. The cathode was constructed by mixing a composite of 60% active material, 15% Super P carbon, 15% CMK-3 mesoporous carbon, and 10% polyvinylidene difluoride (PVDF) binder (percentages by weight) in *N*-methyl-2-pyrrolidone. For the high active mass ratio cells, 80% active material was mixed with 5% Super P carbon, 5% CMK-3 mesoporous carbon, and 10% PVDF binder in the slurry

^a Department of Chemistry and Chemical Biology, Cornell University, Ithaca, New York 14853, United States

† Electronic Supplementary Information (ESI) available: [details of any supplementary information available should be included here]. See DOI: 10.1039/x0xx00000x

composite. The homogeneous mixture was coated onto a carbon paper current collector and dried in a vacuum oven for 2 hours at 60°C followed by 110°C overnight. The dried electrode was cut into disks and assembled into coin cells with a Li metal anode, a dried glass microfiber filter separator and 1 M LiPF₆ in ethylene carbonate (EC): diethyl carbonate (DEC) (1:1 by volume) electrolyte solution.

Characterization Techniques

Fourier transform infrared (FTIR) analysis was done in transmittance mode using a Bruker Tensor II with an attenuated total reflection (ATR) attachment. Differential scanning calorimetry (DSC) measurements were done with a TA Instruments Q1000 using a heat/cool/heat cycle with heats at 20 °C min⁻¹ and cools at 10 °C min⁻¹. Thermogravimetric analysis (TGA) was done on a TA Instrument Q500 at a rate of 10 °C min⁻¹. Images of the polymers were obtained with a Zeiss Gemini 500 scanning electron microscope (SEM). Images were taken with a 1.0 keV working voltage using a 20.0 μm aperture with mixed detection from a high efficiency secondary electron detector and an in-lens detector. A Rigaku Ultima IV x-ray diffractometer was used to obtain powder x-ray diffraction (XRD) spectra for each of the samples. Measurements were conducted with a 40 kV operating voltage and 44 mA current at a scan speed of 2.0 degrees per minute. A BioLogic SP-150 potentiostat was used to collect cyclic voltammetry (CV) and potentiostatic electrochemical impedance spectroscopy (PEIS) measurements. A Neware battery test station was used for galvanostatic charge/discharge tests and galvanostatic intermittent titration technique (GITT) experiments.

Discussion

We recently examined the effect of structural ordering on the charge storage mechanism of organic-based electrode materials.¹⁸ A series of redox active materials based on diphenyl-phenazine (diPh-PZ) exhibited decreased diffusional limitations associated with charge storage with decreased

structural order. The charge transfer kinetics of the most disordered material reflected that of a surface-controlled process. Specifically, the branched polymer network, poly(1,3,5-phenylene-phenazine) (poly(135Ph-PZ)) exhibited fewer diffusion limitations when compared to the linear polymer, poly(phenylene-phenazine) (poly(Ph-PZ)) (Fig. 1a).

We previously reported on the performance of poly(Ph-PZ) as a battery cathode material.¹⁹ The material can undergo two reversible one electron oxidations at each of the tertiary amine units and is charge compensated by the anions present in the electrolyte solution (Fig. S1). The polymeric material exhibited both high capacities (209 mAh g⁻¹) and rate capabilities, retaining 80% of its capacity when discharged at 60 C (a discharge time of one minute). The reduced diffusion limitations and improved theoretical capacity of poly(135Ph-PZ) (232 mAh g⁻¹ vs. 209 mAh g⁻¹ for poly(Ph-PZ); the repeat units used to determine theoretical capacity for each polymer are depicted in Fig. S2) encouraged us to evaluate the polymer network as a cathode material. The rate performances of the two polymers were compared as composites containing 60% active material by weight (Fig. 1b). At 1 A g⁻¹ (approximately 5 C), poly(Ph-PZ) initially delivered an improved capacity, relative to poly(135Ph-PZ) (193 mAh g⁻¹ vs. 184 mAh g⁻¹, respectively), despite its lower theoretical capacity. However, during the first 20 cycles, the capacity of poly(Ph-PZ) decayed more rapidly, becoming slightly lower than that of poly(135Ph-PZ). Surprisingly, when the rate of discharge was increased to 16 A g⁻¹, both materials exhibited approximately 80% capacity retention of their 20th cycle capacity, despite the reduced diffusion limitations in the charge storage kinetics of poly(135Ph-PZ).

When the active material content was increased to 80% in the cathode composite, differences in performance between the polymers became apparent (Fig. S3). At 1 A g⁻¹, poly(Ph-PZ) was still able to deliver 130 mAh g⁻¹, while poly(135Ph-PZ) was limited to 100 mAh g⁻¹. Further, poly(Ph-PZ) retained 67% of its 20th cycle capacity when the rate was increased to 16 A g⁻¹, while poly(135Ph-PZ) retained only 20%. A summary of these results can be found in Table 1. These results suggest that the

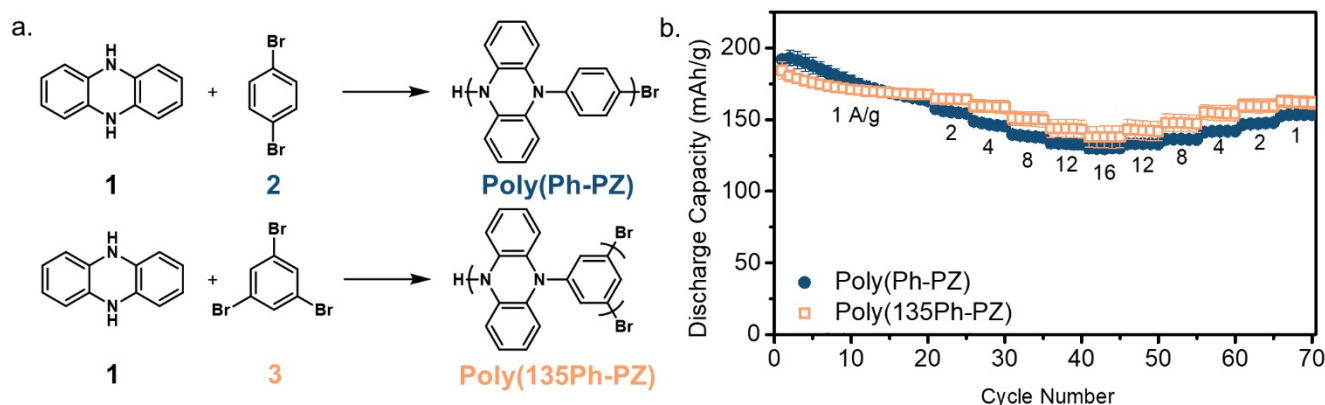


Fig. 1 (a) Schematic of the synthesis of poly(Ph-PZ) (upper) and poly(135Ph-PZ) (lower). (b) Rate performance of poly(Ph-PZ) (blue) and poly(135Ph-PZ) (orange) with 60% active material in the battery composite at discharge rates denoted in the figure. Error bars represent one standard deviation, determined from three or more replicate cells.

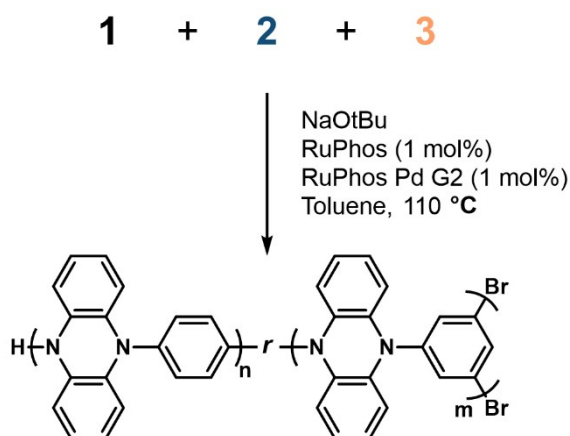
Table 1. Summary of performance metrics of poly(Ph-PZ) and poly(135Ph-PZ).

	Poly(Ph-PZ)	Poly(135Ph-PZ)
Capacity at 1 A g ⁻¹ (60% ^a)	193 mAh g ⁻¹	184 mAh g ⁻¹
Capacity at 16 A g ⁻¹ (60% ^a)	130 mAh g ⁻¹	138 mAh g ⁻¹
Capacity at 1 A g ⁻¹ (80% ^a)	130 mAh g ⁻¹	100 mAh g ⁻¹
Capacity at 1 A g ⁻¹ (80% ^a)	58 mAh g ⁻¹	15 mAh g ⁻¹

^a Percentages describing the weight percent of active material in the cathode composite.

intrinsic conductivity of poly(135Ph-PZ) is lower than that of poly(Ph-PZ) and thus its performance is more limited at high active mass contents.

Inspired by our previous work in which the properties of two co-polymers were improved by the generation of novel ter-polymers, we sought to combine the linking unit of poly(135Ph-PZ) with that of poly(Ph-PZ) to create a new polymer cathode material architecture with optimized performance.¹⁹ Using the Buchwald-Hartwig cross-coupling reaction, 5,10-dihydrophenazine (**1**) was combined with 1,4-dibromobenzene (**2**) and 1,3,5-tribromobenzene (**3**) at the relative molar ratios denoted in Table 2 and shown schematically in Fig. 2. The polymers were characterized using infrared (IR) spectroscopy (Fig. S4). The spectra showed a gradual transition from that of

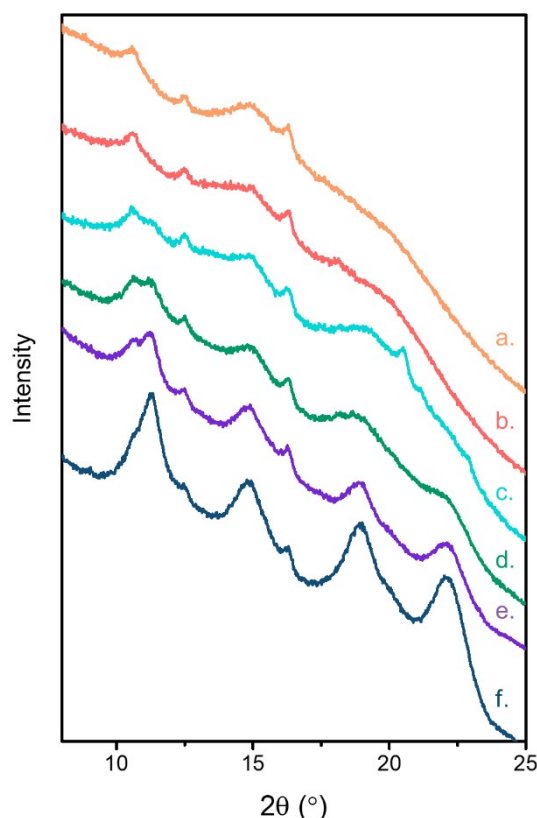
**Fig. 2** Schematic representing the synthesis of ter-polymer samples.**Table 2.** Molar ratios of 5,10-dihydrophenazine (**1**), 1,4-dibromobenzene (**2**), and 1,3,5-tribromobenzene (**3**) used in the Buchwald-Hartwig cross-coupling reaction.

Polymer	1 (mol %)	2 (mol %)	3 (mol %)
Poly(Ph-PZ)	1.0	1.0	0.0
Poly(135Ph-PZ)-10	1.0	0.90	0.07
Poly(135Ph-PZ)-25	1.0	0.75	0.17
Poly(135Ph-PZ)-50	1.0	0.50	0.33
Poly(135Ph-PZ)-75	1.0	0.25	0.50
Poly(135Ph-PZ)	1.0	0.0	0.66

poly(Ph-PZ) to poly(135Ph-PZ) with increased incorporation of **3**. SEM images revealed the unique morphology of each of the studied polymeric materials and identified the particles sizes to be on the order of microns (Fig. S5).

The crystallinity of the polymers was investigated using XRD (Fig. 3). As previously reported, poly(Ph-PZ) exhibits four small, broad peaks at low angles, indicating the existence of some short-range ordering. The peaks at ~19 and 22° correspond to *d* spacings of 4.7 and 4.0 Å, respectively, which are typical of π stacking distances.²⁰⁻²² With increased incorporation of **3**, these peaks broadened and merged into one peak, while the other diffraction peaks subsequently broadened and diminished in amplitude. We ascribe this to a loss in the ordering associated with π stacking interactions between polymer chains resulting from the increased branching in the **3**-rich polymers. The lack of defined peaks suggests an amorphous structure and/or very small domain sizes. Further, the lack of *T_m* or *T_c* in the DSC traces is consistent with the amorphous character of each polymer, indicating that the peaks observed by XRD likely correspond to short-range ordering in the polymer (Fig. S7).

To test their electrochemical properties, each of the polymers was incorporated into a cathode composite with 60% active material by weight and tested in a lithium metal half-cell. The CV profiles of the polymers at 0.25 mV s⁻¹ are shown in Fig. 4. With increased incorporation of **3**, several notable features in the CV profile are evident. First, the formal potential, *E*⁰, of both redox couples increased, ultimately improving both the energy and power densities of the material. Second, the peak

**Fig. 3** XRD spectra of (a) poly(135Ph-PZ), (b) poly(135Ph-PZ)-75, (c) poly(135Ph-PZ)-50, (d) poly(135Ph-PZ)-25, (e) poly(135Ph-PZ)-10, and (f) poly(Ph-PZ)

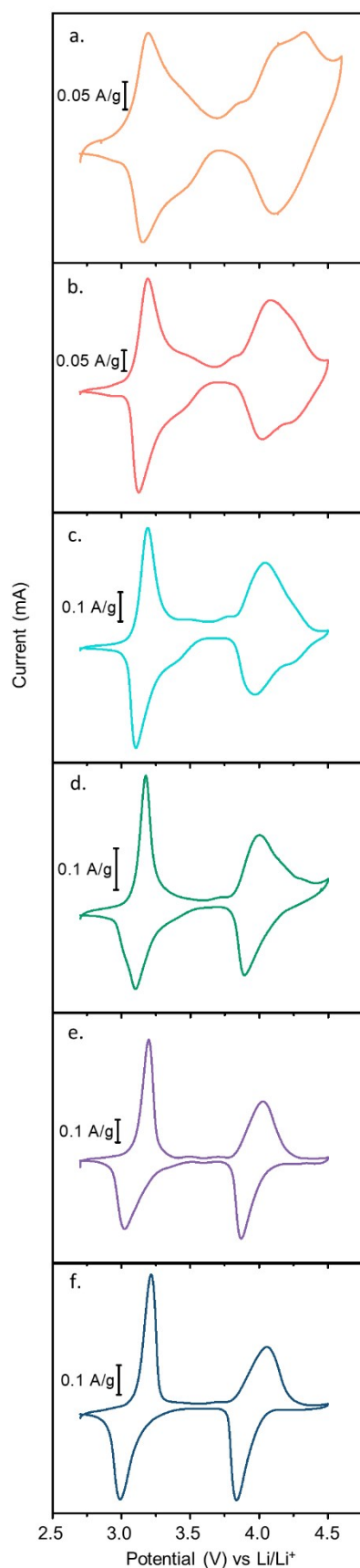


Fig. 4 CV profiles at 0.25 mV s^{-1} in Li metal half cells for (a) poly(135Ph-PZ), (b) poly(135Ph-PZ)-75, (c) poly(135Ph-PZ)-50, (d) poly(135Ph-PZ)-25, (e) poly(135Ph-PZ)-10, and (f) poly(Ph-PZ).

splitting, ΔE_{pk} , for both redox couples decreased, corresponding to an increased energy efficiency. Additionally, the peak broadness increased. These three features are indicative of increasingly repulsive interactions between the redox centers and/or an increase in the number of chemically and spatially distinct redox sites. The reduced polarization and increased cell voltage resulting from this effect are ultimately beneficial to the performance of the electrode material.²³

Examination of the dQ/dV profiles from galvanostatic charge/discharge experiments at 1 A g^{-1} , revealed similar features to the CV profiles along with additional insights with cycling (Fig. S8 and S9). The first charge cycle of poly(Ph-PZ) and

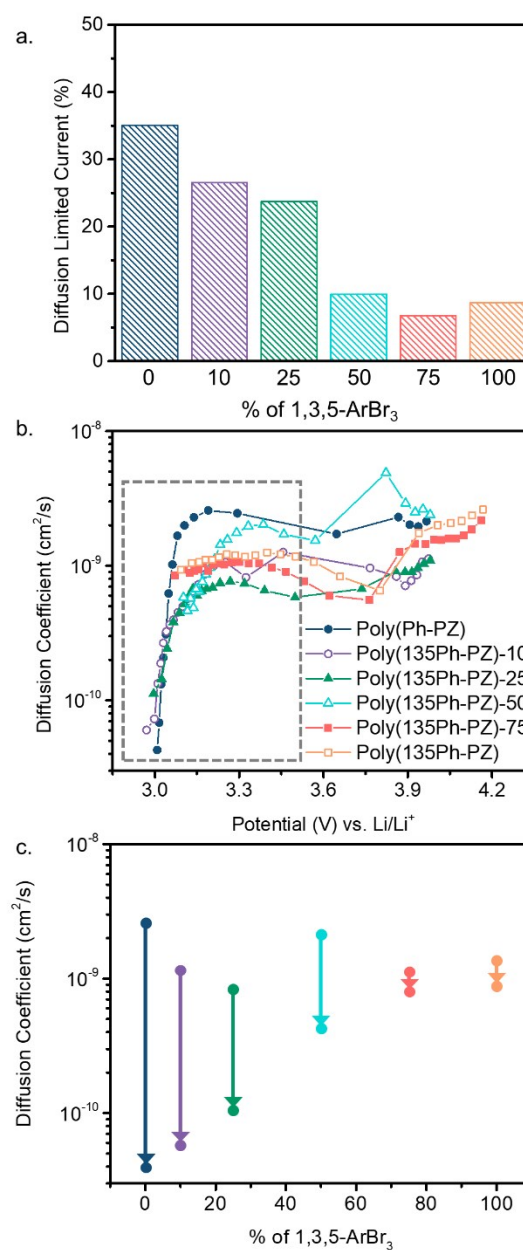


Fig. 5 (a) Percentage of current arising from diffusion limited processes from the cathodic sweep at 0.05 mV s^{-1} with different percentages of incorporated **3**. (b) Diffusion coefficients associated with discharge from GITT. Grey box represents the diffusion coefficients associated with discharge from +1 to neutral. (c) Change in the diffusion coefficient during the reduction from +1 to the neutral state with percentage of incorporated **3**.

poly(135Ph-PZ)-10 (to a slightly lesser extent) required a ~ 730 mV overpotential and a two-step process to fully oxidize the polymers to the +1 state. While in subsequent cycles, the first oxidation of poly(Ph-PZ) and poly(135Ph-PZ)-10 converged to a one-step process, and the observed ΔE_{pk} continued to decrease with cycling. This suggests that the polymers containing higher ratios of **2**, and possessing more ordered structures, undergo an activation type process in the initial cycles, after which the materials exhibit smaller polarizations, more similar to those of poly(135Ph-PZ). The materials containing a high ratio of **3** did not undergo this breaking-in process, and instead, exhibited fast, reversible kinetics throughout cycling.

CVs at low scan rates ($0.05 - 1 \text{ mV s}^{-1}$) can be analysed to determine current, i , arising from diffusive ($i \propto v^{1/2}$) or surface-controlled ($i \propto v$) processes by the following equation²⁴:

$$i = k_1 v + k_2 v^{1/2}$$

where k_1 and k_2 are constants corresponding to the surface-controlled and diffusion-controlled currents, respectively, and v is the scan rate. Fig. 5a displays the percentage of current arising from diffusion-controlled processes during the cathodic sweep at 0.05 mV s^{-1} (the integrated profiles are shown in Fig. S10). In general, the current arising from diffusional processes decreased with increasing incorporation of **3**, indicating increasingly surface-controlled kinetics with increased amorphous character. Poly(135Ph-PZ)-75 exhibited the smallest percentage of diffusion controlled current, which we expect to be beneficial for the rate performance.

To better quantify the rate of diffusion, GITT was used to determine diffusion coefficients throughout the charge/discharge process (Fig. S11 and 5b, respectively).^{25,26} Poly(135Ph-PZ) exhibited exceptionally high diffusion coefficients throughout charge/discharge, on the order of $10^{-9} \text{ cm}^2 \text{ s}^{-1}$, corresponding to the fast transport of hexafluorophosphate anions (PF_6^-) through the polymer. However, in poly(Ph-PZ), the diffusion coefficients dramatically decreased at potentials corresponding to the faradaic events, indicating slower diffusion of ions during the charge-

compensating processes (with the exception of the reduction from the +2 to the +1 state). This effect was especially pronounced during discharge from a +1 charge to the neutral state, where the decrease in the diffusion coefficients spanned two orders of magnitude (Fig. 5c). Increasing the content of **3** in the polymer reduced this drop, such that in poly(135Ph-PZ)-75, the diffusion coefficients exhibited minimum changes throughout charge/discharge, indicating fast diffusion independent of the faradaic events and the accompanying insertion/extraction process.²⁷ We expect this facile diffusion throughout charge/discharge to enable ions to access the entire material, even at high rates.

The electronic conductivity of the materials was evaluated using potentiostatic electrochemical impedance spectroscopy (Figures S12 and 13). The impedance spectra were acquired at 3.6 V to probe the resistance of the polymers in the charged state and avoid complicating the response with the kinetics of the charge transfer reactions (redox conduction). The resistance associated with charge transport in the polymers, derived from fitting the obtained spectra, can be found in Table 3. Poly(135Ph-PZ)-10, -25, and -50 exhibited slightly lower resistance values than poly(Ph-PZ), indicating that a small amount of incorporated **3** appears to improve the electronic conductivity. Poly(135Ph-PZ)-75 and poly(135Ph-PZ) exhibited slightly higher resistance values, which may indicate slower electronic transport.

Encouraged by the improved properties exhibited by the ter-polymers relative to their parent co-polymers, the novel polymers were tested as cathode materials by galvanostatic charge/discharge experiments. The polymers were charged/discharged at 1 A g^{-1} (approximately 5 C) and the resulting profiles are shown in Fig. 6a (charge/discharge curves are plotted separately in Fig. S14). With increased incorporation of **3**, the polarization between the charge/discharge curves decreased, the plateaus became increasingly sloped, and the average working potential increased. The theoretical capacity increased with the ratio of **3** in the polymer. However, the delivered (reversible) capacity increased with increasing **3** only up to poly(135Ph-PZ)-75, after which the capacity decreased.

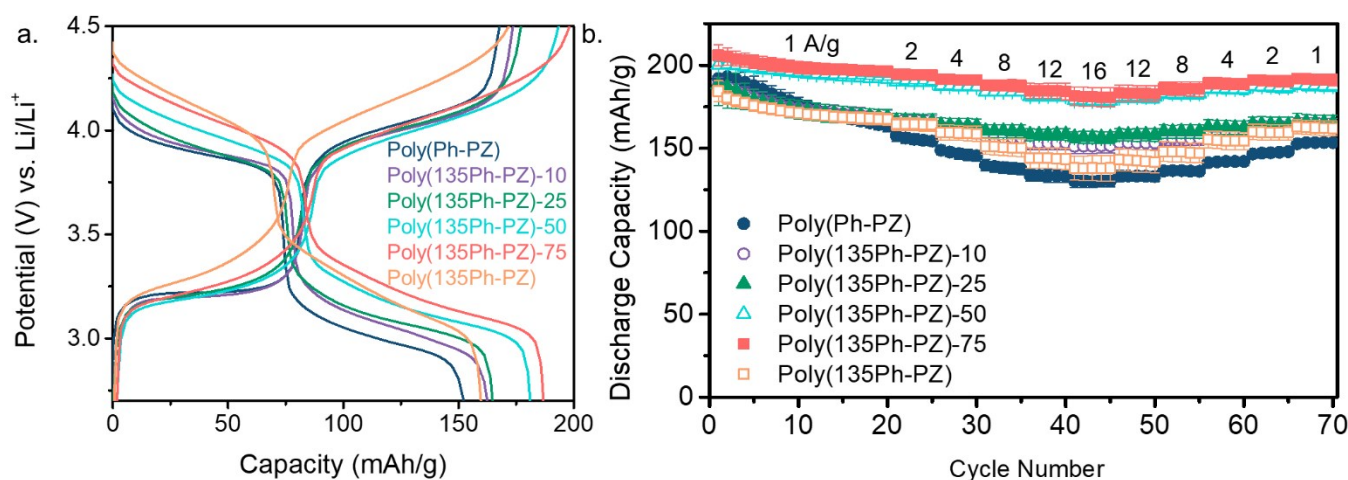


Fig. 6 (a) Galvanostatic charge/discharge profiles of polymers after 20 cycles at 1 A g^{-1} . (b) Rate performance of polymer composites with 60% active material by weight. Rates of discharge indicated above the corresponding rate data. Error bars represent one standard deviation, determined from three or more replicate cells.

Table 3. Charge transport resistances obtained from fitting PEIS spectra at 3.6 V vs. Li/Li⁺.

Polymer	Charge transport resistance [Ω]
Poly(Ph-PZ)	195
Poly(135Ph-PZ)-10	161
Poly(135Ph-PZ)-25	182
Poly(135Ph-PZ)-50	185
Poly(135Ph-PZ)-75	207
Poly(135Ph-PZ)	283

This could be due to insulating regions in the fully cross-linked polymer which are inaccessible during the charge/discharge process or an excess of heavy Br chain ends (not included in the calculation of the theoretical capacity) which are expected to be of higher prevalence in polymers containing a higher content of the tri-functionalized linkers.^{28,29}

The materials were tested for their rate performance (Fig. 6b, summary plot provided in Fig. S15). Excitingly, all the ter-polymers exhibited both improved capacities and capacity retentions relative to the co-polymers. We find that poly(135Ph-PZ)-50 and poly(135Ph-PZ)-75 performed best at high rates. At 16 A g⁻¹, the two polymers delivered 180 mA h g⁻¹, demonstrating a 92% retention of their 1 A g⁻¹ capacities. This represents a 12% improvement in retention and an additional 50 mA h g⁻¹ delivered, relative to poly(135Ph-PZ) and poly(Ph-PZ). These results demonstrate the significance of balancing ionic and electronic conductivity/transport in electrode materials and architectures.

Further, to demonstrate the importance of combining **1**, **2**, and **3** within the polymer structure, we conducted rate tests on a cathode composite in which the active material was composed of a 50-50 blend of poly(Ph-PZ) and poly(135Ph-PZ) (Figure S16). This composite exhibited a rate performance very similar to the parent copolymers, delivering a slightly lower capacity at 1 A g⁻¹ (172 mA h g⁻¹) and retaining slightly more capacity at 16 A g⁻¹ (84% retention). The performance of this 50-50 blend of the two parent copolymers is unable to match that of poly(135Ph-PZ)-50, demonstrating the importance of the copolymerization strategy employed here to effectively tune electronic and ionic transport.

The polymers were next tested for their cycling stability. Each polymer was cycled at 1 A g⁻¹ for 500 cycles. Poly(135Ph-PZ)-75 achieved the highest reversible capacity due to the combination of high electronic conductivity, facile diffusion, and its higher theoretical capacity relative to those with less incorporated **3**. However, poly(135Ph-PZ)-75 and poly(135Ph-PZ) exhibited increased capacity loss with cycling. Due to the higher potentials of the second oxidation in these materials, these cells spend longer times at increasingly anodic potentials where side reactions can occur and cause degradation in the cell.³⁰ We expect that these degradation reactions cause a reduced cycling stability in these materials. To test our hypothesis, poly(135Ph-PZ) was cycled using 4.3 V vs. Li/Li⁺ as the upper cutoff potential in place of the 4.5 V cutoff used in the previous experiments (Fig. S17). Although initially these cells achieved a lower capacity due to incomplete charging, with

continued cycling these cells outperformed the cells of poly(135Ph-PZ) charged to 4.5 V because of the improved cycling stability and capacity retention.

The promising performance of poly(135Ph-PZ)-50 and poly(135Ph-PZ)-75 inspired us to test these materials in a composite with 80% active material by weight. The cells were subjected to the previously employed rate tests and their performances were compared with those of poly(Ph-PZ) and poly(135Ph-PZ) (Fig. 7b). Unfortunately, at the higher active mass loading, poly(135Ph-PZ)-75 dropped to lower capacities than poly(Ph-PZ) at rates above 2 A g⁻¹, likely due to the lower conductivity of the composite with the lowered carbon content. However, poly(135Ph-PZ)-50 exhibited the highest specific capacities at all tested discharge rates. At 1 A g⁻¹, poly(135Ph-PZ)-50 delivered 135 mA h g⁻¹, a 48 mA h g⁻¹ improvement over the capacity delivered by poly(Ph-PZ). At 16 A g⁻¹, while poly(135Ph-PZ)-50 exhibited a slightly reduced capacity retention relative to poly(Ph-PZ) (65% retention vs. 67%, respectively), it delivered an improved capacity of 88 mA h g⁻¹. Combined with the increased average working potential of poly(135Ph-PZ)-50, this capacity corresponds to an

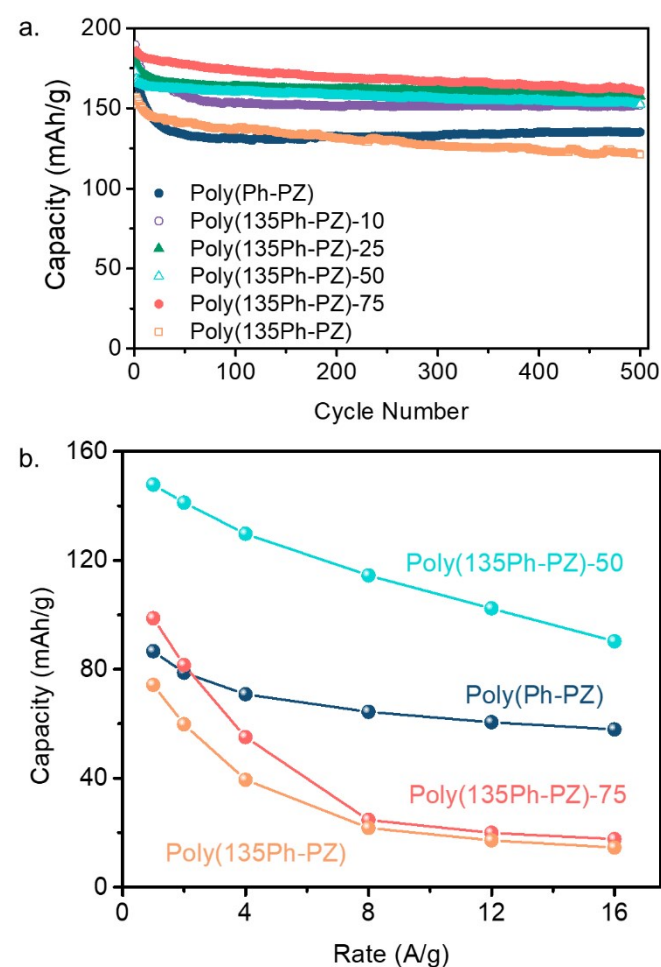


Figure 7 (a) Cycling performance of polymers charged/discharged at 1 A g⁻¹ for 500 cycles with 60% active mass by weight in the cathode composite. (b) Rate capabilities of specific polymers when tested with 80% active mass by weight in the cathode composite.

exceptionally high-power density of 18.1 kW kg⁻¹ when normalized to of the mass of cathode composite.

While the gravimetric energy and power densities of these materials are impressive, it is worth noting that the areal loadings (~0.9 mg of active material per cm²) and the volumetric energy density of the tested materials are low due to the inherently low density of the polymers compared to metal oxide-based electrode materials. Still, the high gravimetric capacity and exceptional rate capabilities of poly(135Ph-PZ)-50 at a high active mass ratio provides a gravimetric energy density competitive with commercial Li-ion battery cathode materials and enhanced power capabilities.

Conclusions

The improved ionic transport of poly(135Ph-PZ) was expected to improve rate performance over that of poly(Ph-PZ). However, the performances of the two polymers were nearly identical due to electronic conductivity limitations in poly(135Ph-PZ). The positive attributes of both polymers inspired a series of ter-polymers which combined the linking units of poly(135Ph-PZ) and poly(Ph-PZ) at different ratios. The synthesized ter-polymers exhibited improved performance over the co-polymers when 60% active material by weight was used in the composite, due to the balanced electronic and ionic transport properties. Poly(135Ph-PZ)-50 demonstrated the most optimized performance of the polymers studied here and was able to deliver an exceptional capacity of 88 mAh g⁻¹ when discharged at 16 A g⁻¹ with 80% active material utilized in the electrode composite. These results demonstrate the importance of balancing both electronic and ionic transport in the design of electrode materials for electrical energy storage applications.

Conflicts of interest

There are no conflicts to declare.

Acknowledgements

C.N.G. and H.D.A would like to thank the National Science Foundation Center for Synthetic Organic Electrosynthesis for funding (CHA-1740656) and Mercedes Benz for funding. L.M.Z. would like to thank the National Science Foundation Graduate Research Fellowship Program for funding (DGE-1650441).

References

- 1 Breakthrough Batteries: Powering the Era of Clean Electrification, https://rmi.org/wp-content/uploads/2019/10/rmi_breakthrough_batteries.pdf, (accessed July 2020).
- 2 J. B. Goodenough and Y. Kim, *Chem. Mater.*, 2010, **22**, 587.
- 3 Y. Tang, Y. Zhang, W. Li, B. Ma and X. Chen, *Chem. Soc. Rev.*, 2015, **44**, 5926.
- 4 M. Armand and J.M. Tarascon, *Nature*, 2009, **451**, 652.
- 5 Y. Liang, Z. Tao and J. Chen, *Adv. Energy Mater.*, 2012, **2**, 742.
- 6 S. Muench, A. Wild, C. Friebe, B. Häupler, T. Janoschka and U.S. Schubert, *Chem. Rev.*, 2016, **116**, 9438.
- 7 M. Yao, K. Kuratani, T. Kojima, N. Takeichi, H. Senoh, T. Kiyobayashi, *Sci. Rep.*, 2014, **4**, 3650.
- 8 M. Armand, *Solid State Ion.*, 1983, **9**, 745.
- 9 Y. Liang, Z. Tao and J. Chen, *Adv. Energy Mater.*, 2012, **2**, 742.
- 10 T. Suga and H. Nishide, in *Stable Radicals: Fundamentals and Applied Aspects of Odd-Electron Compounds*, ed. R.G. Hicks, John Wiley & Sons, 2010, Rechargeable batteries using robust but redox active organic radicals, 507-519.
- 11 Z. Song and H. Zhou, *Energy Envir. Sci.*, 2013, **6**, 2280.
- 12 M. Yao, H. Senoh, S. I. Yamazaki, Z. Siroma, T. Sakai and K. Yasuda, *J. Power Sources*, 2010, **195**, 8336.
- 13 Z. Niu, H. Wu, L. Liu, G. Dai, S. Xiong, Y. Zhao, and X. Zhang, *J. Mater. Chem. A*, 2019, **7**, 10581.
- 14 F. Otteny, V. Perner, D. Wassy, M. Kolek, P. Bieker, M. Winter and B. Esser, *ACS Sustainable Chem. Eng.*, 2019, **8**, 238.
- 15 C. Wang, H. Dong, W. Hu, Y. Liu and D. Zhu, *Chem. Rev.*, 2012, **112**, 2208.
- 16 P. Acker, L. Rzesny, C.F. Marchiori, C.M. Araujo and B. Esser, *Adv. Funct. Mater.*, 2019, **29**, 1906436.
- 17 C. Wang, H. Dong, L. Jiang and W. Hu, *Chem. Soc. Rev.*, 2018, **47**, 422.
- 18 B.M. Peterson, C.N. Gannett, L. Melecio-Zambrano, B.P. Fors and H.D. Abruña, *ACS Appl. Mater. Interfaces*, submitted.
- 19 C.N. Gannett, B. M. Peterson, L. Shen, J. Seok, B. P. Fors, H. D. Abruña, *ChemSusChem*, 2020, **13**, 2428-2435.
- 20 C. Wang, H. Dong, L. Jiang and W. Hu, *Chem. Soc. Rev.*, 2018, **47**, 422.
- 21 M. J. Allen, V.C. Tung and R.B. Kaner, *Chem. Rev.*, 2010, **110**, 132.
- 22 M. Tang, S. Zhu, Z. Liu, C. Jiang, Y. Wu, H. Li, B. Wang, E. Wang, J. Ma and C. Wang, *Chem*, 2018, **4**, 2600.
- 23 H. Angerstein-Kozłowska, J. Klinger and B.E. Conway, *J. Electroanal. Chem. Interfacial Electrochem.*, 1977, **75**, 45.
- 24 T.C. Liu, W.G. Pell, B.E. Conway and S.L. Roberson, *J. Electrochem. Soc.*, 1998, **145**, 1882.
- 25 W. Weppner and R.A. Huggins, *J. Electrochem. Soc.*, 1977, **124**, 1569.
- 26 C.J. Wen and R.A. Huggins, *J. Solid State Chem.*, 1981, **37**, 271.
- 27 S. Zhuo, M. Tang, Y. Wu, Y. Chen, S. Zhu, Q. Wang, C. Xia and C. Wang, *Nanoscale Horiz.*, 2019, **4**, 1092.
- 28 C.R. DeBlase, K. Hernández-Burgos, K.E. Silberstein, G.G. Rodríguez-Calero, R.P. Bisbey, H.D. Abruña and W.R. Dichtel, *ACS Nano*, 2015, **9**, 3178.
- 29 C.R. Mulzer, L. Shen, R.P. Bisbey, J.R. McKone, N. Zhang, H.D. Abruña and W.R. Dichtel, *ACS Cent. Sci.*, 2016, **2**, 667.
- 30 A. Guéguen, D. Streich, M. He, M. Mendez, F.F. Chesneau, P. Novák and E.J. Berg, *J. Electrochem. Soc.*, 2016, **163**, A1095.